archaeometry

Archaeometry ••, •• (2012) ••–•• doi: 10.1111/j.1475-4754.2012.00685.x

AN ARCHAEOMETALLURGICAL STUDY OF 13TH-CENTURY ARROWHEADS AND BOLTS FROM THE CRUSADER CASTLE OF ARSUF/ARSUR*

D. ASHKENAZI†

Faculty of Engineering, Tel Aviv University, Ramat Aviv, 69978, Israel

O. GOLAN

Department of Mechanical Engineering, Afeka Academic College of Engineering, Tel Aviv, 69107, Israel

and O. TAL

Department of Archaeology and Ancient Near Eastern Cultures, Tel Aviv University, Ramat Aviv, 69978, Israel

Selected iron arrowheads and bolts retrieved from the destruction layer of the Crusader castle of Arsur/Arsuf, which was taken down by the Mamluk army (headed by Baybars) in late April 1265, were studied. Being the only site within the boundaries of the Latin Kingdom of Jerusalem that has thus far yielded more than 1200 iron arrowheads, an archaeometallurgical characterization was performed. The aim of this research was to study the warfare methods and manufacturing technologies used by the Mamluk and Crusader armies. Examination included optical microscopy, SEM and SEM–EDS, XPS and microhardness tests. Analysis was performed on both the metallic iron and iron oxides. Ferrous wooden 'fossils', which were found on and within the bolts, were dendroarchaeologically tested. The microstructure analyses show that the weapons were made of wrought iron. These results are correlated with the function of the weapons. The different microstructures of the arrowheads and the bolts indicate dissimilar manufacturing processes. The graphitization of the ropes on the bolts and the oxide phases on their surfaces both provide evidence of high-temperature fire. The ropes support the archaeological findings that these devices were used by the Mamluks to set the Crusader castle on fire.

KEYWORDS: MEDIEVAL IRON ARROWHEADS, MEDIEVAL IRON BOLTS, ARCHAEOMETALLURGY, ARSUR (APOLLONIA-ARSUF), CRUSADERS, MAMLUKS

INTRODUCTION

Arsuf/Arsur (also known as Apollonia) was conquered by Baldwin I of Jerusalem and his Crusader army in 1101 CE. Several decades later, Arsur became the seat of a feudal seigneury that extended over the southern Sharon Plain. The first known lord of the seigneury was a certain Johannes de Arsur. In 1187, Arsur was conquered by the Muslims, but reoccupied by the Crusaders after the battle of Arsuf, where Richard I (Lionheart) of England led the Crusader victory over the army of Saladin on 7 September 1191, during the Third Crusade. In 1207, John of Ibelin (Lord of Beirut) married Melisende of Arsur and became the Lord of Arsur. His son, John of Arsur, inherited the title and passed it down to his son, Balian of Arsur, who, in 1241, built

*Received 8 January 2012; accepted 5 April 2012
†Corresponding author: email dana@eng.tau.ac.il

the walls and castle anew. As danger grew from the expanding Mamluk Empire headed by Sultan Baybars, who had seized power in 1260, it became crucial for a strong and well-organized military order to take over and garrison Arsur. Hence, in 1261, the castle, the town and the entire seigneury of Arsur (*castellum, civitatem et dominium Arsur*) were leased to the Hospitallers by Balian of Ibelin for 4000 besants a year. This act effectively brought an end to the actual lordship of Arsur, although later heirs of the Arsur line of the Ibelins continued to bear the formal title of Lord or Lady of Arsur until the late 14th century CE. The Hospitallers were granted the profits of justice in Arsur in 1263 and according to Muslim sources, in that same year they started to build up a stronghold in the town. This probably meant an eastern enlargement of the walled city, as confirmed by excavation at the site. Baybars considered this act a violation of the treaty that he had just concluded with Crusader leaders.

In mid-March 1265, a large and well-equipped Muslim army under the personal command of Baybars laid siege to Arsur. From the Crusader point of view, Arsur was relatively well prepared. Its city and castle were strongly fortified, well provisioned and defended by some 2000 warriors, about 270 of whom were brothers of the Hospitaller Order. The Muslims' first step was to fill the city wall's moat with wooden beams, but the defenders soon set them ablaze. Then the attackers dug two mines straight towards the castle. They were met with counter-mines and their wooden frame was torched. Baybars then gave the order to simultaneously dig camouflaged access ditches that were carefully planned by his engineers, raise assault ramps in the moat, continuously bombard the city wall with heavy stones thrown by mangonels and constantly harass its defenders with arrows. To inspire his men, the sultan mingled among them, doing all manner of work with his own hands and fighting as one of them. On 26 April 1265, after 40 days of siege, a concerted attack was carried out and the city was taken by storm. The surviving defenders took refuge in the castle and continued to fight with superb courage. However, after three more days of fierce fighting, Muslim warriors took control of part of the castle's fortifications and were able to raise the banners of Islam over the walls. It is that destruction of the castle and the weaponry found therein that are the focus of this paper.

The Hospitallers, after having lost up to 1000 warriors, including 90 knights, asked to surrender on condition that the survivors would be free to leave. Baybars at first agreed but then broke his word, and all of them were taken into slavery. Moreover, he forced the Christian prisoners to participate in the systematic demolition of their own stronghold. The entire site of Arsur was subsequently razed to the ground and left in ruins. This final destruction is largely attested to by thick conflagration layers and ruins that were uncovered in the excavated areas all over the fortified site in general, and in the castle in particular (cf., Roll 1999, 13–17 and fns. 26–37: for the history and archaeology of Arsur and its destruction, with an extensive bibliography, see Tal and Roll 2011; for the conquest of Arsur by Baybars, see Amitai 2005; and for an overview on the castle, see also Roll 2008).

Controlled archaeological excavations in the Crusader town of Arsur and especially in its ruined castle (Fig. 1) have revealed clear evidence of a fierce fight, with the documentation of some 1250 arrowheads and 2750 ballista stones (Raphael and Tepper 2005). All are securely dated to late April 1265, which is the date of the site's destruction by the Mamluks.

Most of the arrowheads bear the same design and are the familiar types of the 12th and 13th centuries (cf., e.g., Jessop 1996); from their frequency at various sites they may be presumed to have served both in Crusader and Muslim bows. They are tanged, pyramid-shaped, rectangular or rhomboid in section, with an average length of 4.5 cm and a maximum width of about 1 cm (Figs 2 (c)–(f) and Fig. 3). Another type, of similar design but with a maximum width of about 3 cm, is also attested in smaller numbers (Fig. 2 (b)). The arrow was made either of reed or wood.

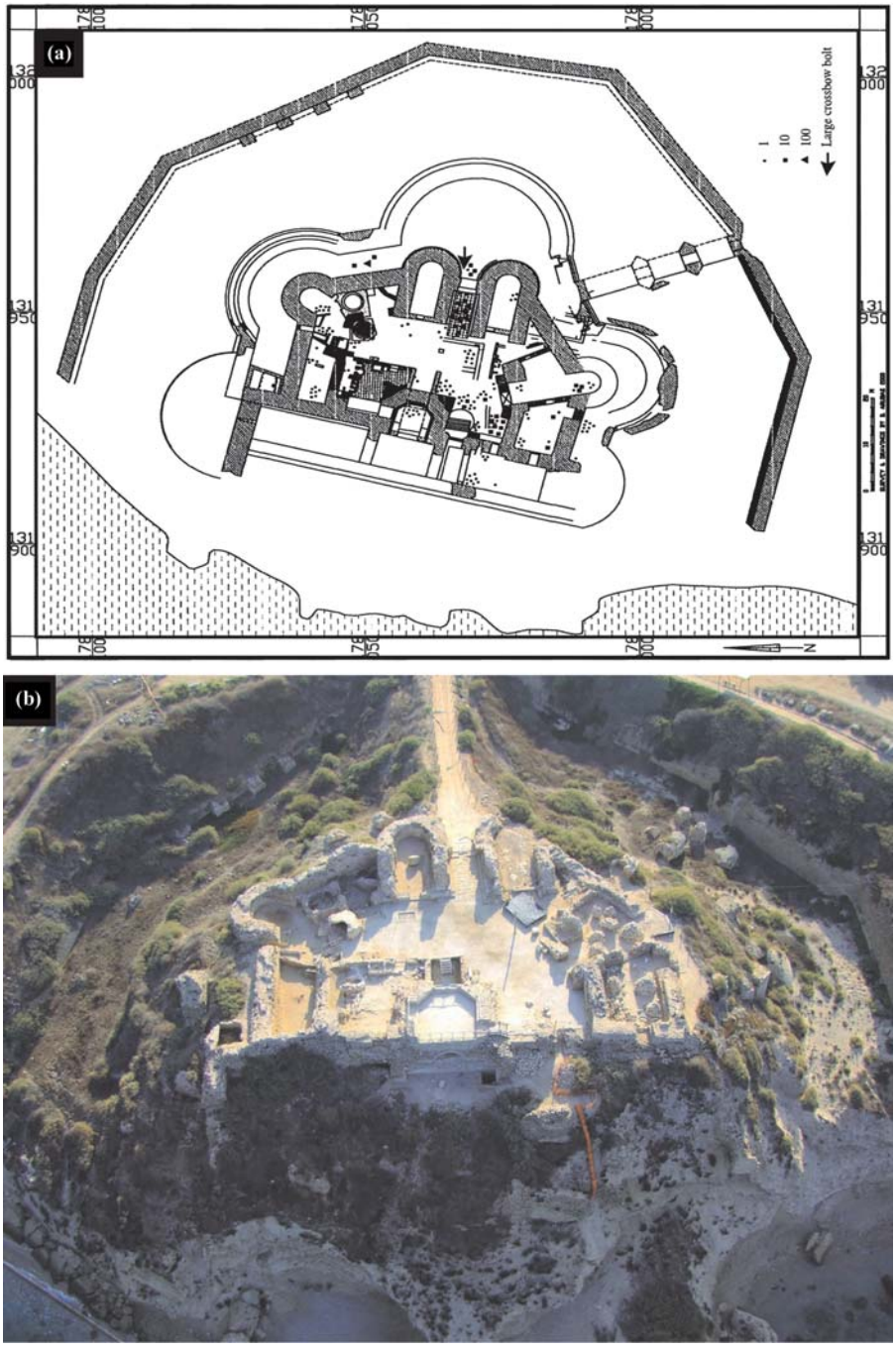

Figure 1 *(a) A plan of the castle of Arsur, showing the distribution of the arrowheads (after Raphael and Tepper 2005); (b) a general view of the site.*

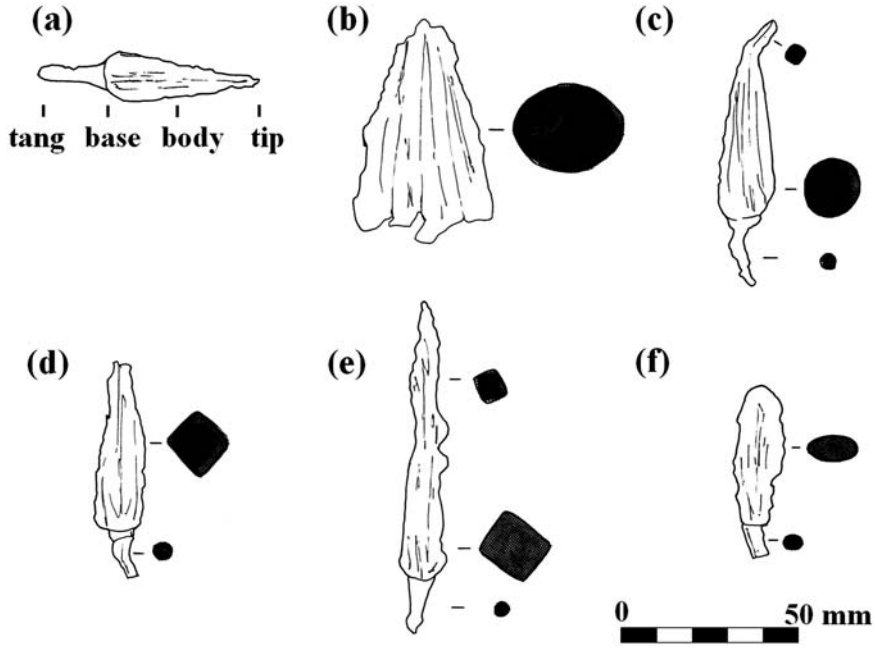

Figure 2 *Typical types of iron arrowheads found at Arsur: (a) the major parts of the arrowheads are the tang, base, body and tip; (b) a wide, pyramid-shaped arrowhead, round in section, with no tang preserved; (c) a tang, pyramid-shaped and round in section; (d, e) a tang, pyramid-shaped and rhomboid in section; (f) a tang, leaf-shaped and lentoid in section.*

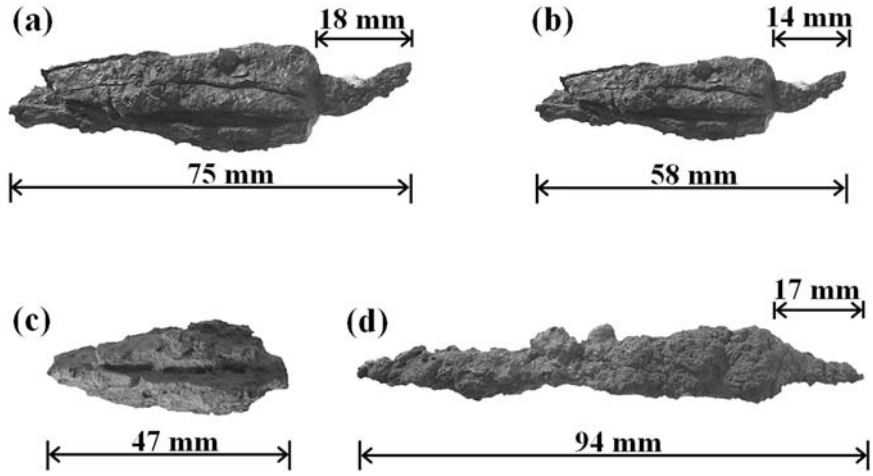

Figure 3 *Thin pyramid-shaped arrowheads from Arsur: (a) A1, rhomboid in section; (b) A2, round in section; (c) A3, rhomboid in section; (d) A4, rhomboid in section.*

In addition, a few leaf-shaped, kite-shaped and flat iron arrowheads were discovered in small numbers (Fig. 2 (f)).

Of special interest are three iron bolts discovered near the gate of the Crusader castle. One is complete (B1) and bears tie marks across its body and some remains of strands of rope, as well as burnt fragments of wood on its tip (Fig. 4). The two other bolts (B2 and B3) are typologically related body fragments (Figs 5 (a) and 5 (b) for B2 and B3, respectively). The three bolts were probably shot out of a bolt-projecting trebuchet towards the gate, in order to set it on fire. More bolts would have been expected to be found in the fosse of the castle if excavated intensively. The use of bolt-projecting trebuchets by the Mamluk army was discussed at some length by Chevedden (2004; for a translation of the military manual written by the Ayyubid writer Murḍā b. ʻAlī b. Murḍā al-Ṭarūsī's, for Saladin in the late 12th century, where the first clearly written record of a counterweight trebuchet appears, see also Cahen 1947–8). Chevedden's evaluation of the contemporary historical sources suggests that the *qarābughrā* played a useful role in most of the major sieges undertaken by the Mamluks in the 13th century (Chevedden 2004, 248).

The complete iron crossbow bolt (B1), as well as one of the fragments (B3), yielded wooden remains in their hollow wedges. Two pieces measuring 0.5–1.0 cm^3 were sampled from the hollow wedges of these corroded bolts for botanical identification by Nili Liphschitz of the Botanical Laboratories, Institute of Archaeology, Tel Aviv University. The samples were treated in absolute ethyl alcohol, dipped in a celloidin – clove oil solution for 24 h, rinsed in absolute ethyl alcohol and transferred to paraffin at 55°C in the oven for 4 weeks. Two blocks were made

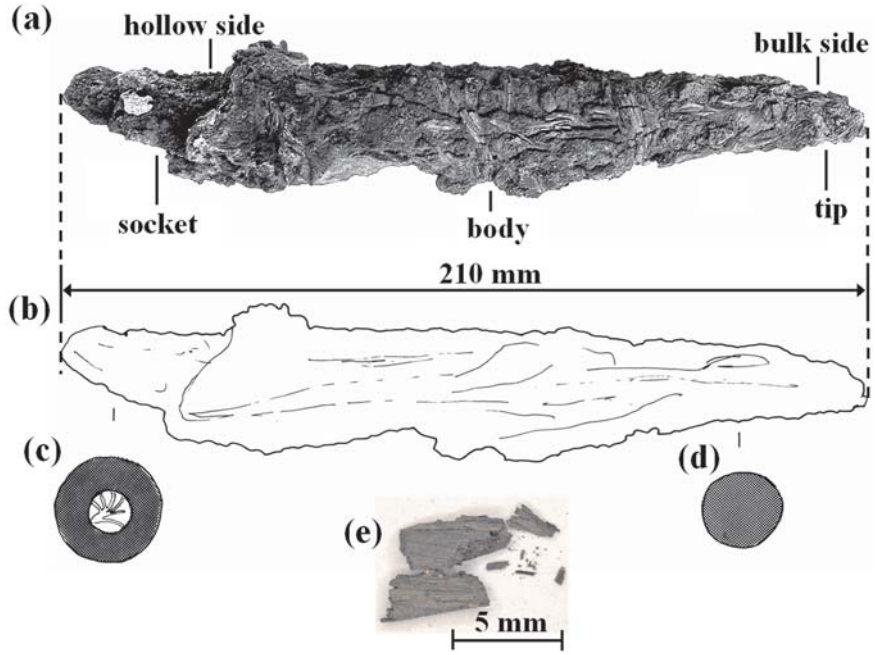

Figure 4 *A complete iron bolt (B1) found at Arsur: (a) a photograph that includes the major parts of the bolt—the hollow base, body and tip; (b) a drawing of the parallel cracks that resulted from the plastic deformation process; (c, d) cross-sections; (e) fossil ropes that were wrapped around the bolt.*

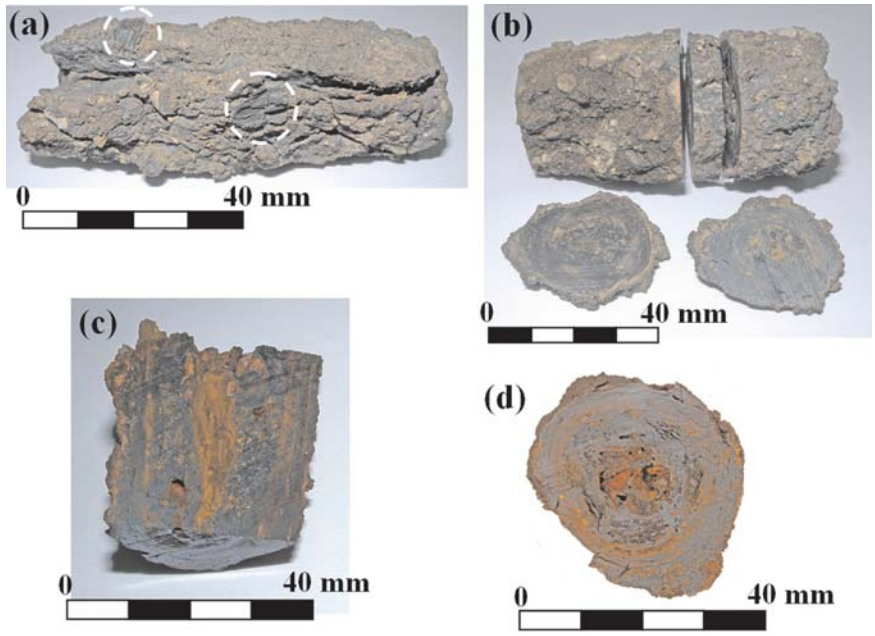

Figure 5 *(a) The broken bolt (B2) from Arsur, showing organic remains and deep cracks parallel to the L direction, as a result of plastic deformation. (b) The slice samples and their locations after removal from the bolt (B3). (c) The L cross-section of the bolt, showing fossil wood (*Pistacia palaestina *[terebinth]) at the central bore. (d) The macrostructure of the slice, revealing circular cracks and rings of orange–brown corrosion.*

in paraffin. Cross, longitudinal and tangential as well as radial sections were prepared for the samples with a microtome. Identification of the tree species, based on the three-dimensional structure of the wood, was made microscopically from these sections. Comparison was made to reference sections prepared from systematically identified recent trees and shrubs and with anatomical atlases. Both samples show that the arrows were made of *Pistacia palaestina* (terebinth), a tree native to the Mediterranean region of Israel. *Quercus calliprinos* (Kermes oak) was the native climax arboreal association that dominated the Mediterranean territory of the land of Israel in antiquity, prior to massive human impact on the environment (Liphschitz 2007, 46–8, 166–9). However, *Pistacia palaestina* trees grew in the Crusader period in the environs of Arsur, and the arrows were apparently made on the site itself.

The present work attempts to fill this gap between the historical data of the site and the technological knowledge, as revealed by the material itself. Information regarding the ancient iron arrowheads and bolts, including their microstructure and composition, as well as their manufacturing technologies, can provide significant information on their use, their origin and the technological skills of the Mamluk and Crusader armies.

TECHNICAL BACKGROUND

The knowledge behind ancient iron and steel weapons has long fascinated archaeologists and scientists. Interaction between cultures, such as trade connections and wars, as well as varying technological abilities, can be examined through the material itself. Numerous papers have

utilized typological and archaeometallurgical methods to study the microstructure, material properties and manufacturing process of such weapons, of which mechanical properties such as high yield strength and good fracture toughness are required, as expected by modern observers (e.g., Jones 1992; Pense 2000; Wadsworth and Lesuer 2000; Perttula 2001, 2004; Blyth and Atkins 2002; Abdu and Gordon 2004; Ehrenreich *et al*. 2005; Nicodemi *et al*. 2005; Hošek and Košta 2006; Mapelli *et al*. 2007; Barella *et al*. 2008; Balos *et al*. 2009). Mapelli *et al*. (2007) used archaeometallurgical methods to study medieval iron sword production during the 12th century CE. The sword that they examined, which was found in northern Italy, had suffered from oxidation on the external part of the weapon. It was concluded that the sword had been made using friction-welding of steel strips (Mapelli *et al*. 2007).

In the 13th century, the manufacturing process of relatively pure iron included a reduction process at a temperature of around 1200°C, which turned the iron ore into a spongy matter called 'bloom' (Tylecote 1962, 46–57; Eliyahu *et al*. 2011). At the next stage, the bloom was hammered in order to join the porous iron by forge-welding and to remove the slags from the ingot bulk. The result was a 'wrought iron', which was a malleable and ductile material (Tylecote and Black 1980; Eliyahu *et al*. 2011).

Archaeological iron weapons buried for a long period in soil environments usually suffer from intensive corrosion. When the iron is exposed to normal or oxidizing atmospheres, it forms iron oxide layers that change the nature of the surface/environment interface. The major iron oxides are hematite (α-Fe_2O_3), magnetite (Fe_3O_4), maghemite (γ-Fe_2O_3), wüstite (FeO), β-Fe_2O_3 and ε-Fe_2O_3 (Cornell and Schwertmann 2003). Goethite is an isolating phase, whereas lepidocrocite is the active phase in the corrosion process. Magnetite forms at high temperatures, but also at room temperature or during soil corrosion processes, whereas wüstite forms at high temperatures only. With time, changes occur in the iron oxide corrosion product—from lepidocrocite to goethite (dark zones), and at high temperatures it converts into stable phases such as maghemite (light grey) or hematite (Balasubramaniam *et al*. 2003). A range of ferrous artefacts, several hundred years old, that had undergone atmospheric corrosion were examined by Dillmann *et al*. (2004). The main corrosion phases observed in the alloy were lepidocrocite, goethite, akaganeite and magnetite. Cracks in various orientations were also observed. The long-term corrosion stability of iron artefacts with varying thicknesses of rust layers and cracks in various orientations was analysed by Yoshikawa *et al*. (2008). The main phases observed were goethite, lepidocrocite, magnetite, hydrated iron oxide and non-ferrous darker slag in the matrix. Balos *et al*. (2009) examined fourth-century CE Roman blades and concluded that they were iron 'fossils', in which the iron was transformed under high temperatures into iron oxide consisting of FeO and Fe_3O_4, with a typical hardness of 425 HV.

The present research discusses the possible manufacturing process of ancient iron weapons, their raw materials and their chemical composition by examining the iron metallic segments and their structural relationships to the surrounding iron oxide environment.

EXPERIMENTAL METHODS AND TESTS

The current investigation uses archaeometallurgical methods to offer some answers to questions relating to arrowheads and bolts retrieved from the Crusader castle of Arsur, such as the warfare methods and manufacturing technologies used by the Mamluk and Crusader armies. The medieval iron arrowheads and bolts were first observed under a stereo microscope looking for iron, revealing massive degradation processes. The coastal environment of the castle is typified by a highly saline and humid atmosphere that was detrimental to the iron. In such

conditions, metal detector and radiography examinations are not very useful. In such a situation, the best solution was to sacrifice several of the weapons.

The metallurgical examination (summarized in Table 1) included optical microscopy (OM), scanning electron microscopy (SEM) with energy-dispersive spectroscopy (SEM–EDS), X-ray photoelectron spectroscopy (XPS) and microhardness tests. Nine objects were selected for this study: six iron arrowheads, referred to as A1–A6, and three iron bolts, referred to as B1–B3. All came from the castle's gate area (Locus 2884; Basket 28848), where high concentrations of arrowheads were revealed; the find spot of the intact bolt (B1) is shown in Figure 1 (a). The major parts of the medieval arrowheads and bolts are shown in Figures 2 and 4, respectively. Arrowheads A1, A2, A3 and A4 are shown in Figures 3 (a)–(d), respectively. The complete iron bolt, B1, is shown in Figure 4, and the two broken bolts, B2 and B3, are shown in Figures 5 (a) and 5 (b), respectively. The white circle in Figure 5 (a) shows the fossil ropes. In order to perform metallographic examinations of the arrowheads and bolts, samples were cut and mounted in Bakelite at a temperature of 180°C under a pressure of 20 bar in the transversal (T) and longitudinal (L) directions (according to the ASTM-E3 standard). Metallographic specimens A5 and A6 are shown in Figures 6 (a) and 7 (a), respectively. The surface was prepared by grinding the mounted samples with SiC paper (grade 240–600 grit), polishing them with alumina paste (5–0.05 μm) and, lastly, polishing with 0.05 μm colloidal silica suspension pastes. The samples were rinsed in an ultrasonic bath and then cleaned with ethanol and dried. They were then etched with nital acid (97 vol% alcohol and 3 vol% HNO_3). All samples were attracted to magnets to test their ferromagnetic strength. First, the samples were observed under a stereo microscope up to 50× magnification, and then the samples were observed by OM up to 1000× magnification (BF and DF, using a Zeiss Axio Scope A1 microscope). Following the metallographic examination, microhardness tests were performed (for both metal and oxide), using the Vickers microhardness

Table 1 *A description of each artefact and the analysis performed*

Object	*Type*	*Locus*	*Description*	*OM*	*HV*	*SEM*	*EDS*	*XPS*
A1	Arrowhead	AP-Area F, 1999, L. 2824, B. 28448/4	Complete; iron oxide with cracks	+				+
A2	Arrowhead	AP-Area F, 1999, L. 2824, B. 28448/5	Complete; iron oxide with cracks	+				+
A3	Arrowhead	AP-Area F, 1999, L. 2835/B	Complete; iron oxide with cracks	+				
A4	Arrowhead	AP-Area F, 1999, L. 2835/A	Broken (tang is missing); iron oxide with cracks	+	+			
A5	Arrowhead	AP-Area F, 1999, L. 2824/A	Broken (head is missing); bent, fairly well preserved; green surface corrosion	+	+	+	+	
A6	Arrowhead	AP-Area F, 1999, L. 2824/B	Broken (head is missing); bent, fairly well preserved; green surface corrosion	+	+	+	+	
B1	Bolt	AP-G-28, Area F, 2002, L. 2824, B. 28448/A	Complete; iron oxide with cracks	+		+	+	
B2	Bolt	AP-G-28, Area F, 2002, L. 2824, B. 28448/B	Broken, iron oxide with cracks	+	+			+
B3	Bolt	AP-G-28, Area F, 2002, L. 2824, B. 28448/C	Broken; iron oxide with cracks	+		+	+	+

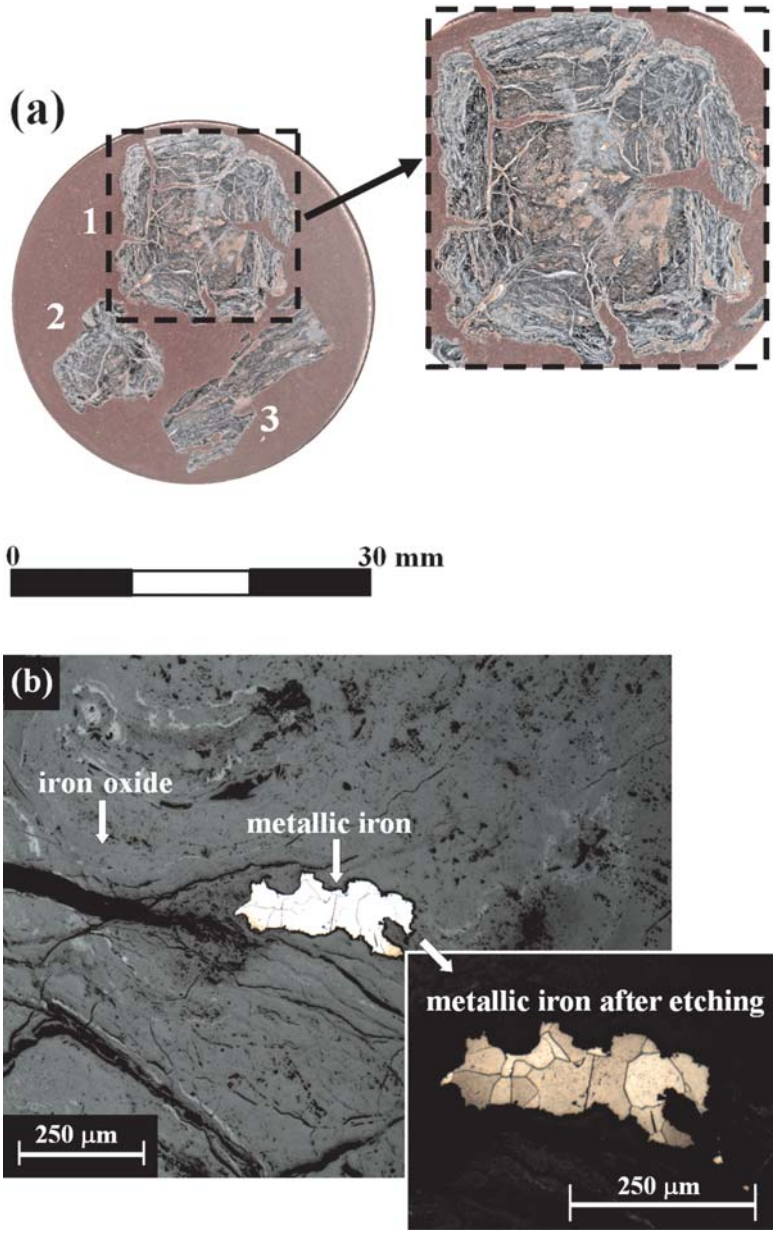

Figure 6 *A metallographic cross-section of arrowhead A5 after etching, revealing: (a) the metallographic specimen, showing the original slightly rectangular shape of the base (1), tip (2) and tang (3) parts of the arrowhead; (b) marbled texture with cracks and an α-iron phase at the arrowhead's tip (OM, T cross-sections); (c) the interface between the α-iron grains and the iron oxide layer at the arrowhead's base, including inclusions (SEM, T cross-sections); (d) the EDS chemical analysis of the inclusions, revealing the presence of a fayalite particle phase; (e) a metallographic T cross-section (SEM) of the iron oxide rectangular base, revealing 'bow-like' curved deformation lines with dark and bright iron oxides caused by forging.*

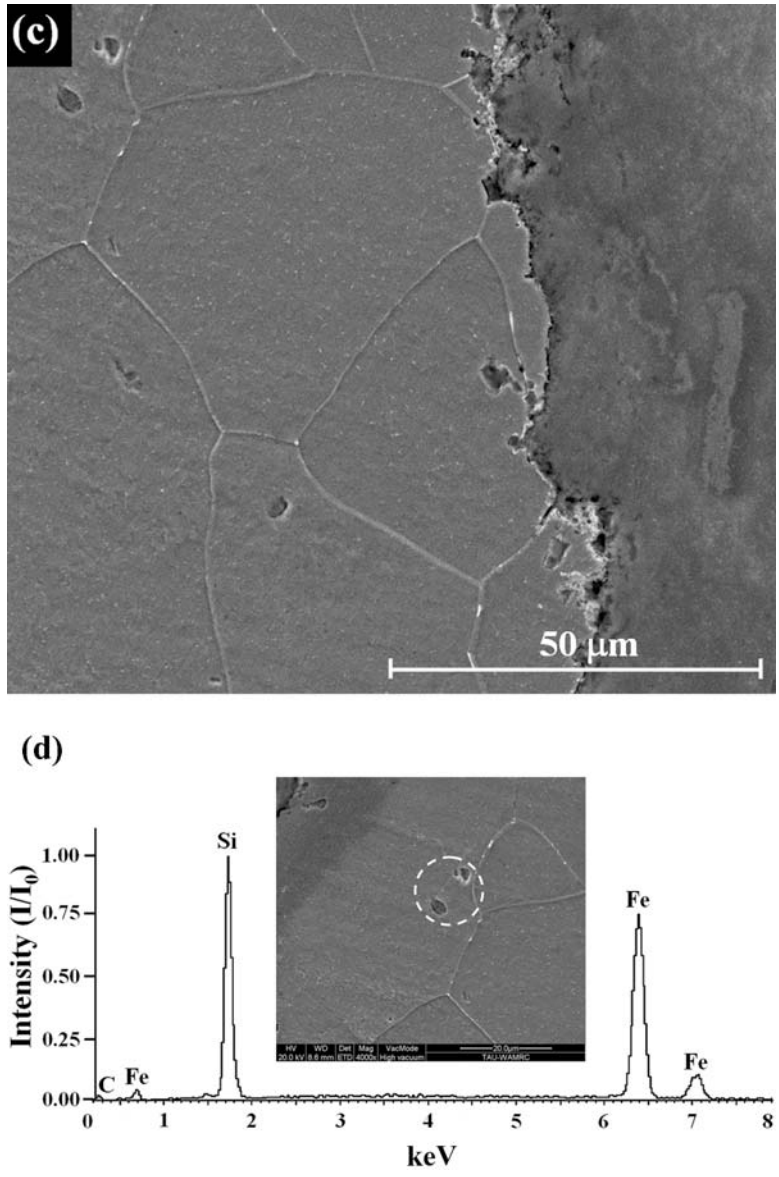

Figure 6—*continued*.

test method (Future-Tech, Microhardness tester, FM-700e) with a diamond indenter employing a 0.025–0.1 kilogram-force (kgf) load, in order to reveal more about the manufacturing process from the mechanical properties.

The surface morphology and composition were examined by SEM and SEM–EDS, using an environmental scanning electron microscope (ESEM), in order to discover more about the manufacturing process from the metallographic observations and the chemical composition. The samples were analysed using an FEI Quanta 200FEG ESEM in high-vacuum mode

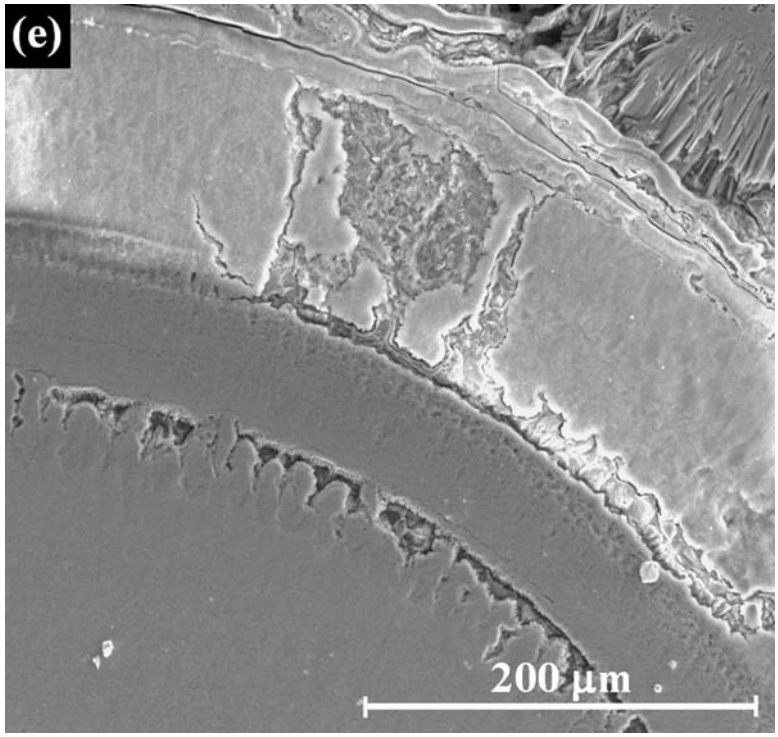

Figure 6—*continued*.

(10^{-5} mbar), with an Everhart–Thonley secondary electron (SE) detector and an accelerating voltage of 20 kV. Chemical element composition was analysed using energy-dispersive spectroscopy (EDS) with an Si(Li) liquid-cooled Oxford X-ray detector (which detects elements down to boron).

The XPS measurements were carried out in addition to the SEM–EDS in order to expose light elements (such as nitrogen) in low concentrations (less then 1 wt%). The XPS measurements were performed in UHV (2.5×10^{-10} Torr base pressure) using a 5600 Multi-Technique System (PHI, USA). The samples, 10×10 mm^2 in size, were measured in the transverse sections. They were irradiated with an Al–K_α monochromated source (1486.6 eV) and the escaping electrons were analysed by a spherical capacitor analyser, using the 0.8 mm slit aperture. Ten minutes of sputtering was sufficient to bring the samples to bulk conditions (~2000 Å under the surface). However, the samples were analysed at the surface (survey spectrum) and after 10 and 20 min of sputtering, they were cleaned with a 4 kV Ar^+ ion gun (the sputter rate was ~43 Å min^{-1} on the SiO_2/Si reference sample).

RESULTS

The surface textures of the weapons were marbled, with areas of dark and light iron oxide, and some orange corroded rust along the cracks. All weapons were ferromagnetic, which signifies the presence of metallic iron or iron oxides (magnetite and maghemite). Iron metallic segments were

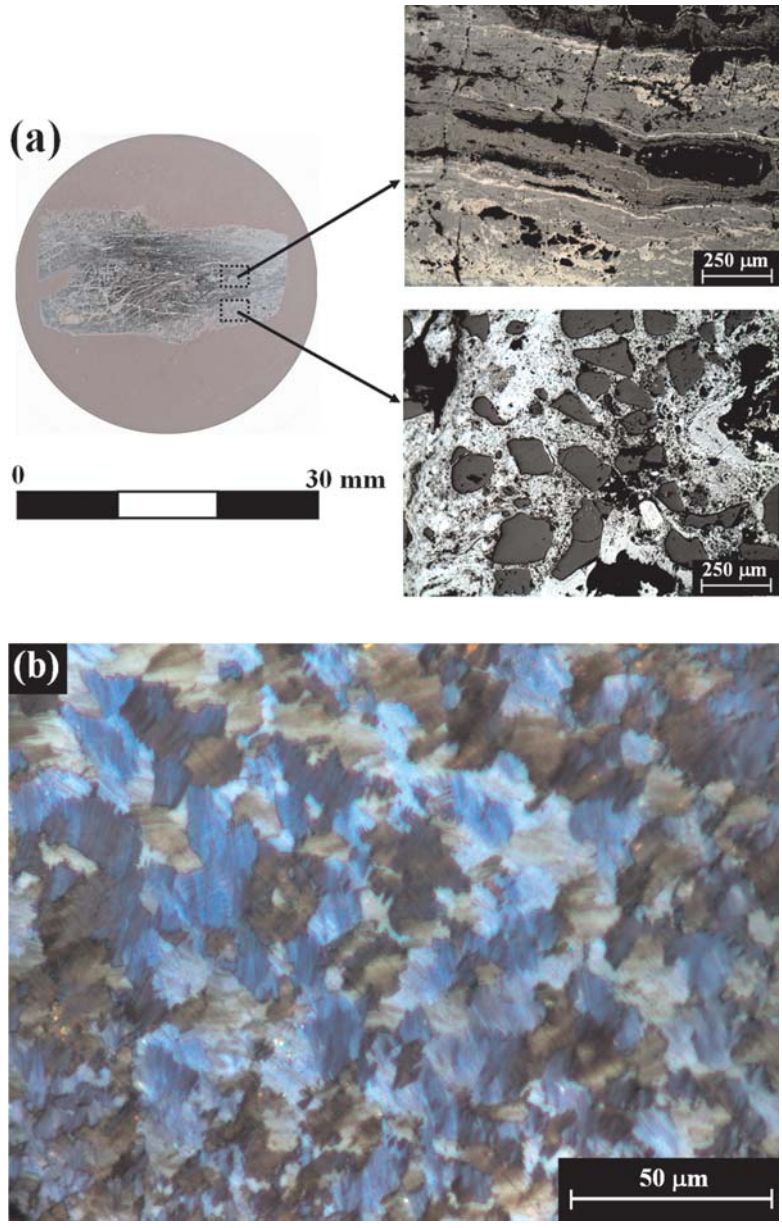

Figure 7 *A metallographic L cross-section (OM) of arrowhead A6 after etching, revealing: (a) cracks, pores and discontinuous texture at the centre of the arrowhead and quartz particles near the external surface of the arrowhead (in the outer part of the corrosion crust, which has developed over the original surface of the arrowhead); (b) magnetite oxides, which had preserved the original iron austenite grains, and are evidence of thermal exposure (observed under polarized light).*

Table 2 *ESEM–EDS results (values in wt% and at%), using Quanta 200 ESEM FEG from FEI*

Specimen		*Compositions (wt%)*						
		Fe	*O*	*Si*	*C*	*Ca*	*Cl*	*Al*
A5 (tang, iron island)	wt%	100.0	–	–	–	–	–	–
	at%	100.0	–	–	–	–	–	–
A5 (tang, iron oxide)	wt%	87.9	12.1	–	–	–	–	–
	at%	67.6	32.4	–	–	–	–	–
A5 (base, iron oxide)	wt%	77.3	13.1	–	5.0	4.6	–	–
	at%	50.6	30.0	–	15.1	4.3	–	–
A5 (base, iron oxide)	wt%	80.1	12.0	–	5.6	2.3	–	–
	at%	53.0	27.6	–	17.3	2.1	–	–
A5 (base, inclusion 1)	wt%	67.5	–	26.5	6.0	–	–	–
	at%	45.6	–	35.5	18.9	–	–	–
A5 (base, inclusion 2)	wt%	13.7	26.2	60.1	–	–	–	–
	at%	6.1	40.8	53.1	–	–	–	–
A5 (base, crystalline oxide structure)	wt%	85.8	8.1	–	–	–	–	6.1
	at%	67.7	22.3	–	–	–	–	10.0
A6 (core, iron oxide)	wt%	81.4	18.6	–	–	–	–	–
	at%	55.6	44.4	–	–	–	–	–
A6 (external surface particles, sample 1)	wt%	–	38.9	61.1	–	–	–	–
	at%	–	52.8	47.2	–	–	–	–
A6 (external surface matrix, sample 1)	wt%	79.7	17.9	1.5	–	–	–	0.9
	at%	54.2	42.5	2.0	–	–	–	1.3
A6 (external surface particles, sample 2)	wt%	–	43.5	56.5	–	–	–	–
	at%	–	56.5	42.5	–	–	–	–
A6 (tang, inclusion 1)	wt%	80.6	–	19.4	–	–	–	–
	at%	67.6	–	32.4	–	–	–	–
B1 (wood rope)	wt%	73.3	15.4	2.0	7.5	1.8	–	–
	at%	43.6	32.0	2.4	20.6	1.4	–	–
B1 (wood rope)	wt%	70.1	18.7	2.0	6.7	1.3	0.6	0.6
	at%	40.2	37.4	2.3	17.8	1.0	0.6	0.7
B3 (hollow base, wooden socket region)	wt%	84.5	11.8	–	3.1	0.6	–	–
	at%	60.0	29.4	–	10.0	0.6	–	–
B3 (hollow base, wooden socket region)	wt%	82.5	17.5	–	–	–	–	–
	at%	57.5	42.5	–	–	–	–	–
B3 (hollow base, wooden socket region)	wt%	80.7	14.3	–	3.6	0.8	0.6	–
	at%	54.0	33.4	–	11.2	0.8	0.6	–

Less than 1 wt% C could not be identified by ESEM–EDS.

observed and tested. The elemental analysis of the weapons is summarized in Table 2 for SEM–EDS and Table 3 for XPS. The mechanical properties of the metallic iron are given in Table 4.

Analyses of the arrowheads

Metallic iron segments surrounded by iron oxides were observed in all arrowheads, as also reported by Neff *et al*. (2005). Macroscopic parallel cracks presented in all arrowheads, as shown in Figure 2. Those parallel cracks followed deformation lines of the original shape that had been

Table 3 *XPS results (values in at%) after 10 and 20 min of sputtering, using the 5600 Multi-Technique System (PHI, USA)*

Specimen	*Sputtering time (min)*	*Compositions (at%)*						
		Fe	*O*	*C*	*Ca*	*Mg*	*N*	*Cl*
A1 arrowhead	10	49.5	47.5	1.4	0.7	0.4	0.4	0.1
	20	53.5	44.2	0.9	0.6	0.5	0.3	–
A2 arrowhead	10	51.0	44.4	3.6	0.7	–	0.3	–
	20	55.7	41.5	1.9	0.6	–	0.3	–
B2 bolt	10	51.2	46.4	1.7	0.5	0.2	–	–
	20	53.2	45.4	0.7	0.4	0.3	–	–
B3 bolt	10	55.5	41.2	2.8	0.5	–	–	–
	20	57.7	40.9	1.0	0.4	–	–	–

created during manufacturing and were probably caused by residual stresses. All arrowheads underwent extensive plastic deformation, due to hot-working, which resulted in thermal residual stresses, as shown by the presence of massive cracks. Some of the cracks may result from corrosion preferentially travelling along the residual contour lines and slag inclusions.

The marbled texture of the oxides is evidence of a wrought-iron manufacturing process, where the initial bloom was hammered and compacted into heterogeneous material when iron pieces were forge-welded together.

The SEM–EDS elemental analysis of the arrowheads revealed an extensive presence of Fe and O, but also elements such as Si, C, Ca and Al (Table 2). The XPS chemical analysis of the arrowheads revealed an extensive presence of Fe and O, as well as elements such as C, Ca, Mg, N and Cl (Table 3). Elements such as Si, Ca, Mg and Al are common in soil.

The α-iron mechanical properties of the arrowheads are summarized in Table 4. The mechanical properties of the α-iron display relatively low microhardness values, with an average of 117 HV for arrowhead A4, 112 HV for A5 and 122 HV for A6. These values are equivalent to UTS values of 388 MPa, 372 MPa and 402 MPa, respectively. The relatively low microhardness values of the α-iron (ferrite) are in accordance with a cold-working (CW) process of about 3–19% CW. The cold-working process strengthens the metal during the manufacturing process.

The medium grey iron oxide phase displays average values of microhardness ranging between 389.2 ± 87.5 HV (A4 arrowhead, tip) and 453.8 ± 97.1 HV (A4 arrowhead, tang), which according to others (Balos *et al*. 2009) could match wüstite and magnetite phases, where wüstite is a high-temperature oxide that cannot occur during the normal corrosion process.

Observation of metallographic cross-sections of arrowhead A5 under OM and SEM (after etching) revealed bright-shiny iron islands with α-ferrite grains (Fig. 6), surrounded by an iron oxide marbled texture and many cracks. Stereo microscope observation of the A5 arrowhead revealed that the original cross-sections of the base and tip were rectangular, as revealed from the contours (Fig. 6 (a)). Ferrite grains between 20 and 80 μm in size were observed at the arrowhead's tip (Fig. 6 (b), T cross-sections, OM) and base (Fig. 6 (c), T cross-sections, SEM). The absence of elongated grains may result from the observation at the perpendicular direction to the cold-working process or from the manufacturing process of the weapons by folding the iron foils.

The SEM–EDS analysis of the tang of arrowhead A5 revealed an elemental composition of Fe, O, C, Ca and Al (Table 2). The EDS analysis of the metallic iron in the tang revealed the presence

Table 4 *The mechanical properties of the metallic material residues*

Specimen	*Vickers hardness number, HV**				*Rockwell B hardness, 100-kgf (HRB)†*	*Approximate tensile strength (MPa)‡*	*Type of processing and treatment§*	*Phases*
	Min.	*Max.*	*Average*	*SD*				
A4 (base, T, area 1)	84.2	147.1	128.6	20.0	71.4	422.7	Cold-worked (19%)	α-Ferrite
A4 (base, T, area 2)	101.2	134.6	114.4	13.2	63.0	378.2	Cold-worked (7%)	α-Ferrite
A4 (tip, T, area 1)	104.0	136.3	117.0	13.0	64.9	386.4	Cold-worked (8%)	α-Ferrite
A4 (tip, T, area 2)	85.2	109.6	102.6	9.9	52.9	341.3	Annealed	α-Ferrite
A4 (tang, L, area 1)	106.3	127.9	115.9	9.0	64.1	382.9	Cold-worked (7%)	α-Ferrite
A4 (tang, L, area 2)	104.1	149.5	127.7	12.7	71.2	419.8	Cold-worked (18%)	α-Ferrite
A5 (base, T, area 1)	98.4	135.5	111.4	13.3	60.8	368.8	Annealed/cold-worked (3%)	α-Ferrite
A5 (base, T, area 2)	90.5	143.6	113.4	16.7	62.3	375.1	Annealed/cold-worked (4%)	α-Ferrite
A6 (body, L)	102.1	167.1	126.3	19.9	70.5	415.5	Cold-worked (12%)	α-Ferrite
A6 (body, L)	92.0	147.8	118.1	21.7	65.6	389.8	Cold-worked (8%)	α-Ferrite

*Vickers (HV) microhardness test using the Future-Tech Microhardness tester (FM-700e), with a diamond indenter employing a 0.025 kgf load.

†Values follow the ASTM E 140-02 Standard for non-austenitic steels.

‡Ultimate tensile strength equivalents, according to ASM (1990a).

§Per cent cold-working equivalents, according to ASM (1990b).

of α-iron Fe (Table 2), with some inclusions at the base of the arrowhead (Fig. 6 (d)). The EDS elemental analyses of the inclusions (Table 2) revealed the presence of Fe, Si, C and O. These inclusions were identified as fayalite particles. The metallographic examination of the iron oxides revealed rounded deformation lines with dark and bright iron oxides caused by forging, at the rectangular base (Fig. 6 (e), SEM, T cross-section).

Metallographic examination of arrowhead A6 (L cross-section, OM after etching) revealed cracks and quartz particles near the external surface (Fig. 7 (a)). The examination of the iron oxides revealed a rounded structure; probably resulting from the hammering that was an integral part of the bloomery process. Measurements of the arrowhead iron ferrite grains revealed sizes between 20 and 80 μm. The SEM–EDS examination of the quartz particles on the external surface of the arrowhead revealed silicon oxide particles composed of Si and O surrounded by an iron oxide matrix containing Fe and O (Table 2 and Fig. 7 (a)). Magnetite oxides, which had preserved the original iron austenite grains (OM differential polarization, Fig. 7 (b)), are evidence for thermal exposure, especially high-temperature fire, which would have resulted from the conflagration in the castle.

Analyses of the bolts

The original cross-sections of all three bolts (B1, B2 and B3) were circular, as shown in Figures 4 (B1) and 5 (b)–(d) (B3). Deep macroscopic cracks were observed in all bolts, as shown in Figure 4 for bolt B1 and in Figure 5 (a) for bolt B2. Those cracks are parallel to the longitudinal direction (parallel to the length of the bolt) and could be a result of the plastic deformation process. The forging (hot-working) process could generate directional residual thermal stresses and enhance the growth of cracks during the corrosion process. Segments of ropes were observed on the external surfaces of the bolts, as shown in Figures 4 (a) and 5 (a).

Contrary to the arrowheads, the ferromagnetism of the bolts was weak. This physical phenomenon is demonstrated by the different kinds of α-iron distribution. Very small amounts of metallic iron residues were detected in the bolts. Furthermore, the α-ferrite grains were found only at the forge-welding interfaces (Fig. 8 (a)). An additional difference between the arrowheads and the bolts was the observation of laminar oxide interlayers in the bolts (Fig. 8 (b)). The bolts' microstructure was characterized by fine laminar morphology and homogeneous parallel layers in most of the bulk. Chemical analysis (SEM–EDS) of the bolts revealed an extensive presence of Fe and O, but also elements such as Si, C, Ca and Cl (Table 2). The XPS chemical analysis of the bolts also revealed an extensive presence of Fe and O, as well as elements such as C, Ca and Mg (Table 3). The absence of nitrogen in the bolt samples is very significant and can distinguish the arrowheads from the bolts.

Macroscopic observation of bolt B1 revealed segments of organic ropes on the surfaces of the artefact (Figs 4 (a) and 4 (e)). These ropes were found in 'fossilized' condition; that is, a rigid, ferrous oxide was present that preserved the original structure of the vegetative tissue. Stereomicroscopic images of the 'fossil' rope segments are shown in Figure 4 (e). SEM observation of these 'fossil' ropes, which were found on the external surfaces of the bolts, exposed the cell tissue (Fig. 9 (a)). Chemical analysis (SEM–EDS) of the 'fossil' ropes (Table 2 and Fig. 9 (b)) revealed the presence of C, Ca, Cl, Si and Al, as well as Fe and O. The high amount of carbon in the ropes probably resulted from the organic tissues, where iron diffused into the tissues during the process of hydro-corrosion that took place after the fire and carbonized the ropes.

Macroscopic and microscopic examination of bolt B2 revealed an organic wooden stem 'fossil' in the central, intact bore of the bolt socket (Fig. 5 (a)). Like the ropes, the stem was also

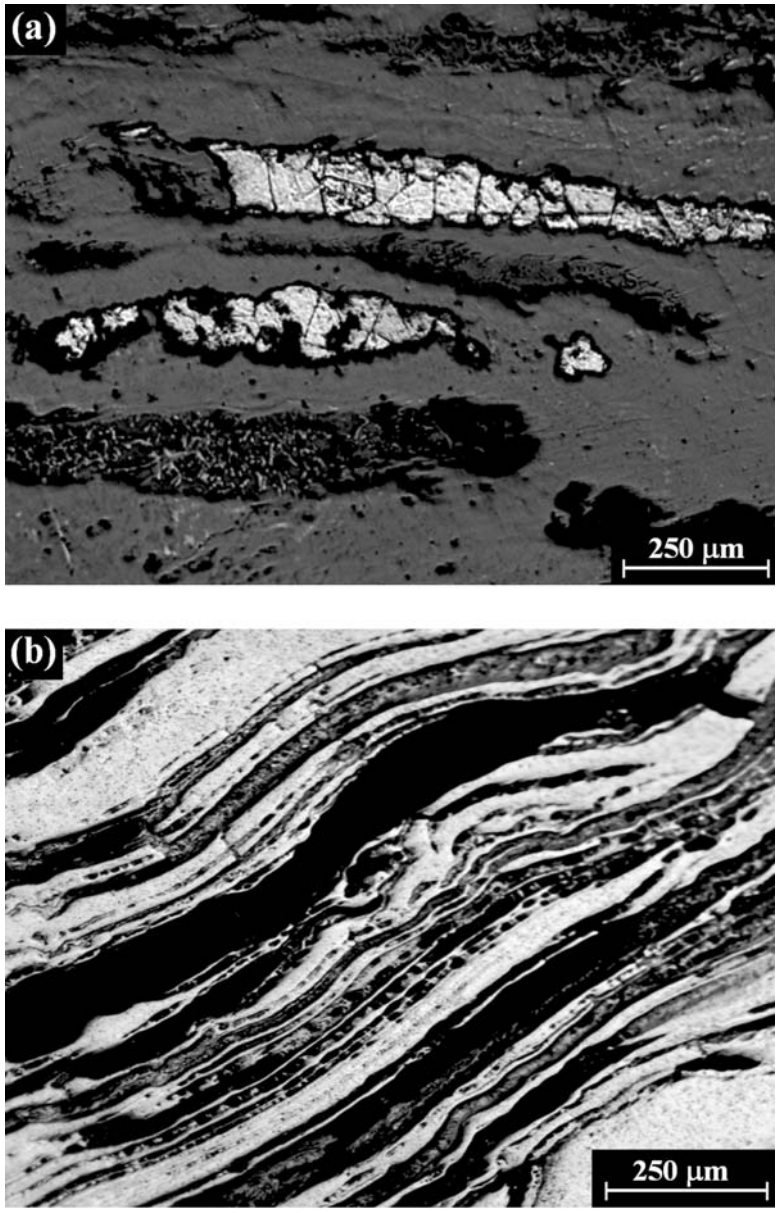

Figure 8 *A metallographic (OM) cross-section of the two broken bolts: (a) bolt B2 after etching reveals α-ferrite grains on the forge-welded interfaces; (b) bolt B3 reveals the laminar structure of the iron oxides.*

found 'fossilized', with a rigid, ferrous skeleton. The features of the secondary vascular tissue were used to assist in identifying the tree species by means of dendroarchaeological analysis. The SEM observation of the secondary xylem in the transverse plane revealed the vessels (tracheids) and the diffuse-porous tissue of the wood (Fig. 10 (a)). Observation of the radial plane revealed the xylem rays and the fibre structure (Fig. 10 (b)). These features are typical of *Pistacia palaestina*.

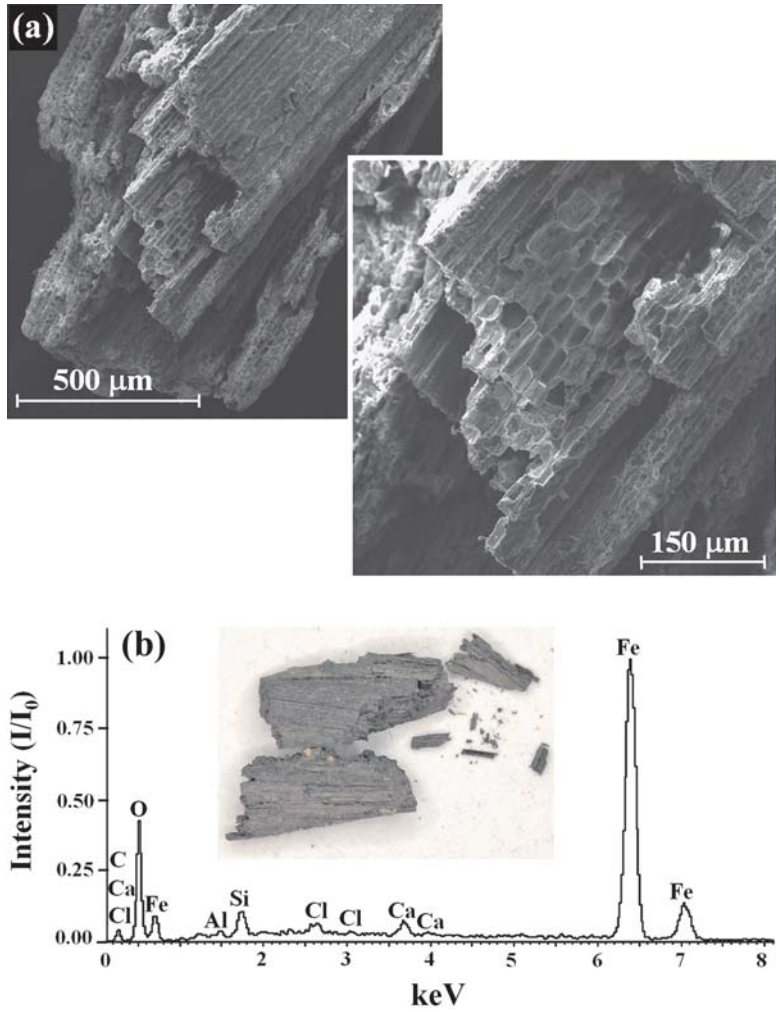

Figure 9 *The residue ropes, which were found on the external surfaces of the bolts: (a) tissue cells (SEM); (b) the ferrous fossil ropes, which when analysed by EDS revealed the presence of C, Ca, Cl and Fe.*

The SEM–EDS analysis of the 'fossilized' wooden stem of bolt B3 (Table 2) revealed organic and soil elements such as C, Ca and Cl, as well as Fe and O. The large quantity of carbon is suggestive of soot remains from the organic tissue.

Observations of bolt B2's metallographic L cross-sections (OM, after etching) revealed bright metallic α-iron grains, with an average size of 50–60 μm (Fig. 8 (a)) and laminar iron oxides with cracks. The metallic iron residues are located only at the forge-welding interfaces (Fig. 8 (a)). These interfaces lead to apertures between the adjacent layers in which the forge-welding process caused the iron particles to be trapped.

Observation of the third bolt (B3, Fig. 5 (b)) by OM and SEM microscopy revealed laminar iron and iron oxide layers, with numerous forge-welding interfaces (Fig. 8 (b)). Quartz particles surrounded by iron oxide were observed adjacent to peripheral surfaces.

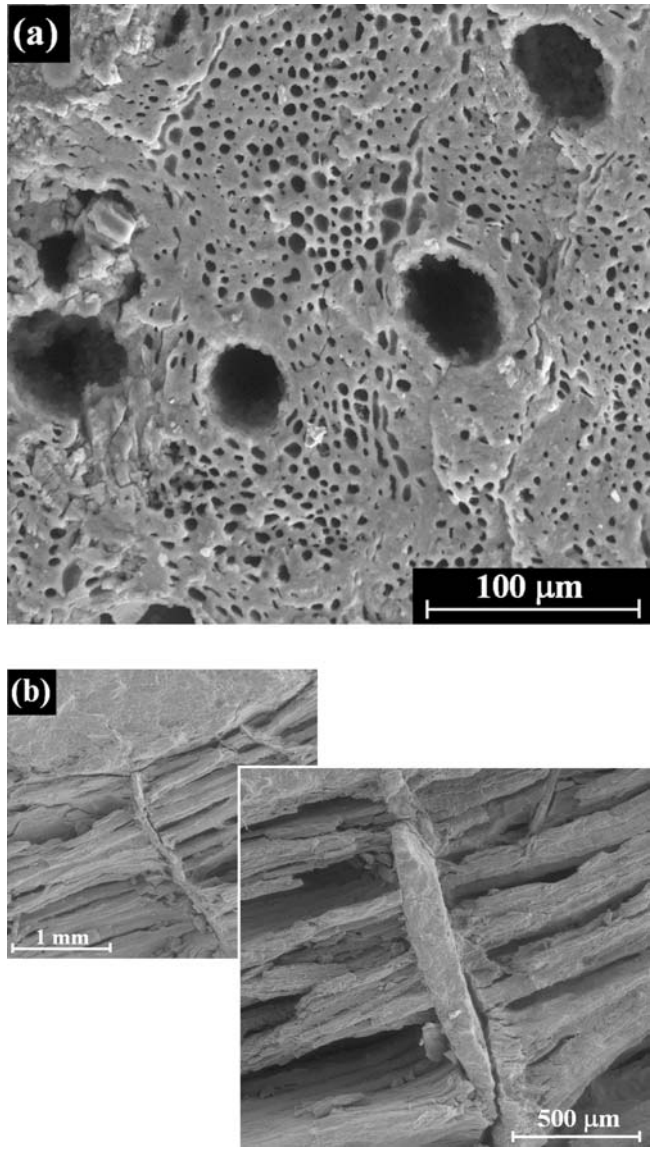

Figure 10 *SEM micrographs of the 'wooden fossils' in the central bore of the bolt: (a) vessels in the vascular tissue of the secondary xylem (transverse plane); (b) the fibres and xylem rays in the radial plane.*

DISCUSSION

Selected iron arrowheads and bolts retrieved from the Crusader castle of Arsur, which was captured by the Mamluk army in late April 1265, were studied using archaeometallurgical methods. All arrowheads and bolts were made of wrought iron, without carburization treatments, and were shaped by hot-working processes. The results indicate two different groups of manufacturing processes. No evidence of steel was found, such as carbonization or heat-treatments. In

contrast to other weaponry, such as swords or daggers (Mapelli *et al*. 2007), the functional features of these arrowheads and bolts do not require aggressive strengthening mechanisms. Consequently, our arrowheads and bolts were made of a single phase consisting of ductile α-iron (ferrite), which could not be strengthened by heat-treatments, but rather only by strain-hardening through a cold-working process. The lack of carbon in all samples indicates that all the weapons were made from raw materials and were not reprocessed from carbon steels. Cementation surface treatments were also not found. The microstructure integrated with the mechanical properties indicates that the blacksmiths worked according to the following sequence: (1) bloomery refining of the iron from its ore; (2) forge-welding and hot-working by hammering; and (3) cold-working as a finishing process.

Evidence of the bloomery process, which resulted in a heterogeneous microstructure, was observed in all the arrowheads, and was recognized from their contour lines. The finishing of the arrowheads by cold-working was demonstrated by the values of the mechanical properties. A small amount of cold-working causes minimal strain-hardening or residual stress, which consequently acts as a slight driving force in the corrosion process. The distribution of dispersed metallic iron within the bulk materials of the weapons is evidence of such a process.

The dissimilar microstructure and distribution of the metallic iron indicate that the bolts and the arrowheads were made using different manufacturing processes. In contrast to the arrowheads, the bolts were characterized by a laminated microstructure that paralleled the contour lines of the artefacts. The layers and the interspaces were very thin and uniform. Numerous metallic iron remains were found between the layers, among the forge-welded interfaces. This typical microstructure results from a meticulous manufacturing process that can be achieved by laminated forge-welding at moderate temperatures. If the temperature is not high enough for recrystallization, two phenomena could occur: (1) high residual stresses; and (2) peeling off of the contact surfaces. A high level of residual stresses aggressively accelerates the corrosion rate of the iron layers (Jones 2003). In contrast, lack of ductility at this insufficient temperature causes the contact interfaces to peel off and iron particles to form. These particles produced a lack of residual stresses and protected the material from additional corrosion. Despite the wider diameters of the bolts (comparing with that of the arrowheads), only minor quantities of metallic remnants were found among the forge-welded interfaces.

The differing technologies used for the arrowheads and bolts single out two dissimilar groups of weaponry manufactured by individual groups of blacksmiths. Although the two different technologies may suggest use by two different armies—for example, the bolts by the Mamluks and the arrowheads by the Crusaders—the evidence that all the weapons were unearthed in the castle's gate area implies that both the bolts and arrowheads were used by the Mamluks. Furthermore, the six arrowheads studied were arbitrarily selected out of some 1250 specimens, and are of three different types, each with its own distinct archaeometallurgical characterization. Given these facts, the idea that they were primarily used by the defenders (i.e., the Crusaders) seems statistically unsound.

The typical microstructure of the weapons was specified by numerous isolated inclusions that were dispersed throughout the cross-sections. The presence of fayalite (Fe_2SiO_4), which is a typical slag inclusion, results from the bloom production and indicates that removal by hammering of the brittle oxides or slag from the bloom was not perfect (Caterina *et al*. 2008). Other widespread inclusions were silica (quartz) particles, which were found predominantly near the external surface of the arrowheads. The source of the quartz particles is the coastal ground, whose primary component is beach sand. Ferrous hydro-oxides penetrated into the adjacent ground,

consolidated the particles and created a composite material made of quartz particles surrounded by a ferrous matrix. The sand sediments migrated along the weapons' cracks and were trapped there.

The present study agrees with the archaeological and historical evidence of the castle's destruction in a fierce conflagration. The main evidence for such a high-temperature fire was the presence of magnetite grains, which preserved the original iron austenite grains resulting from exposure to high temperatures. The initial iron austenite grains were gradually oxidized into magnetite oxides, preserving the original microstructure of the metal. The nature of this phenomenon requires high-temperature, prolonged exposure and combustion conditions (Schwertmann and Cornell 2000). The high-temperature fire contributed to the preservation of the artefacts, due to the protective properties of the oxide layers.

The residue of ropes found on the external surfaces of the bolts supports the archaeological supposition that the Mamluk army fired the bolts at the gate of the Crusader castle, and that the bolts were intended to penetrate the metal sheets over the wooden doors, lodging in the doors and igniting them. Numerous iron nails and pieces of metal sheets found in the gate area corroborate this reconstruction. The substantial ferrous 'fossil' ropes that bound bolt B1 may indicate that their primary function was to ignite wooden elements in the castle. The graphitization of the ropes and the oxide phases on the surface are evidence of thermal exposure, especially high-temperature fire. The ferrous ropes were created by a diffusion mechanism, where the iron penetrated the cell tissue and replaced the organic elements over time. The rigid ferrous oxide skeleton preserved the original structure of the 'fossil' plant tissues. The same mechanism was responsible for the wooden 'fossil' stem at the central bore of the bolts' sockets.

The link between the metal texture, due to hammering, and the oxide texture warrants future study. Further examination, including micro-Raman spectroscopy to identify the structure of the corrosion products, and EBSD studies of the texture of the corrosion products—which are beyond the scope of this paper—also warrants future study.

CONCLUSIONS

The present archaeometallurgical study compares different weapons that were found in the excavation of the Crusader castle of Arsur. The metallurgical examinations utilized various methods in order to reveal the weapons' composition, microstructure, mechanical properties and manufacturing process. All arrowheads and bolts were made of wrought iron, without carburization or heat-treatments, and were shaped by hot-working processes. The results indicate two different groups of manufacturing processes. The arrowheads were shaped by particle hammering, using high-temperature forge-welding, resulting in minor residual stresses and a large quantity of metallic remains. The different technique by which the bolts were manufactured resulted in a small amount of metallic remnants preserved only at the forge-welded interfaces. The dissimilarities between the arrowheads and the bolts are due to the differences between a moderate-temperature manufacturing process and a fine lamellar forge-welding process, which caused stress-relieved iron flakes, which remained trapped between the stressed layers. The fact that all of the arrowheads and bolts were found in the castle's gate zone suggests that they were used by the Mamluk army. The substantial ferrous 'fossil' ropes that bound the intact bolt may indicate that their primary function was to ignite the wooden elements of the castle. Evidence of thermal exposure, especially to high-temperature fire, fully supports the archaeological and historical data on the destruction of the castle in a fierce conflagration.

ACKNOWLEDGEMENTS

The authors wish to thank Nili Liphschitz from the Institute of Archaeology of Tel Aviv University, Roni Shneck from the Materials Department of Ben-Gurion University and Mario Levinstein from the School of Mechanical Engineering of Tel Aviv University for their assistance.

REFERENCES

Abdu, B., and Gordon, R., 2004, Iron artifacts from the land of Kush, *Journal of Archaeological Science*, **31**, 979–98.

Amitai, R., 2005, The conquest of Arsuf by Baybars: political and military aspects, *Mamluk Studies Review*, **9**, 61–83.

ASM, 1990a, *Metals handbook*, 10th edn, vol. 1: *Properties and selection: irons, steels, and high-performance alloys*, ASM, Materials Park, OH.

ASM, 1990b, *Metals handbook*, 10th edn, vol. 14: *Forming and forging*, ASM, Materials Park, OH.

Balasubramaniam, R., Ramesh Kumar, A. V., and Dillmann, P., 2003, Characterization of rust on ancient Indian iron, *Current Science*, **85**(11), 1546–55.

Balos, S., Benscoter, A., and Pense, A., 2009, Roman mystery iron blades from Serbia, *Materials Characterization*, **60**, 271–6.

Barella, S., Mapelli, C., and Nicodemi, W., 2008, A leap into the beginning of the Metal Age: recrystallization and carburizing, *La Metallurgia Italiana*, **100**(April), 9–16.

Blyth, P. H., and Atkins, A. G., 2002, Stabbing of metal sheets by a triangular knife—an archaeological investigation, *International Journal of Impact Engineering*, **27**, 459–73.

Cahen, C., 1947–8, Un traite d'armurerie pour Saladin, *Bulletin d'Études Orientales*, **12**, 103–63.

Caterina, I., Maurizio, T., and Giuseppe, S., 2008, Archaeometallurgy in Messina: iron slag from a dig at block P, laboratory analyses and interpretation, *Mediterranean Archaeology and Archaeometry*, **8**(1), 49–60.

Chevedden, P. E., 2004, Black camels and blazing bolts: the bolt-projecting trebuchet in the Mamluk army, *Mamluk Studies Review*, **8**, 227–77.

Cornell, R. M., and Schwertmann, U., 2003, *The iron oxides: structure, properties, reactions, occurrences and uses*, Wiley-VCH, Weinheim.

Dillmann, P. H., Mazaudier, F., and Hoerle, S., 2004, Advances in understanding atmospheric corrosion in iron, I. Rust characterisation of ancient ferrous artifacts exposed to indoor atmospheric corrosion, *Corrosion Science*, **46**, 1401–29.

Ehrenreich, R. M., Hamilton, E., and Nash, S. K., 2005, Far from barbaric: re-assessing the sophistication of Merovingian metalworking, *JOM*, **57**(8), 51–5.

Eliyahu, E., Barkai, O., Goren, Y., Eliaz, N., Kahanov, Y., and Ashkenazi, D., 2011, The iron anchors from the Tantura F shipwreck: typological and metallurgical analyses, *Journal of Archaeological Science*, **38**(2), 233–45.

Hošek, J., and Košta, J., 2006, Metallography of the 9th century sword of a great Moravian nobleman buried in Mikulice (grave no. 580), *Metallugija—Journal of Metallurgy*, Association of Metallurgical Engineers in Serbia (AME), Broj, **2–3**(12), 199–206.

Jessop, O., 1996, A new artefact typology for the study of medieval arrowheads, *Medieval Archaeology*, **40**, 192–205.

Jones, P. N., 1992, The metallography and relative effectiveness of arrowheads and armor during the Middle Ages, *Materials Characterization*, **29**, 111–17.

Jones, R. H., 2003, Stress-corrosion cracking, in *Corrosion: fundamentals, testing, and protection* (eds. S. D. Cramer and B. S. Covinos), 879–936, ASM Metals Handbook 13A, ASM International, Materials Park, OH.

Liphschitz, N., 2007, *Timber in ancient Israel: dendroarchaeology and dendrochronology*, Monograph Series 26, Institute of Archaeology, Tel Aviv University, Tel Aviv.

Mapelli, C., Nicodemi, W., and Riva, R. F., 2007, Microstructural investigation on a medieval sword produced in 12th century AD, *ISIJ International*, **47**(7), 1050–7.

Neff, D., Dillmann, P., Bellot-Gurlet, L., and Beranger, G., 2005, Corrosion of iron archaeological artefacts in soil: characterization of the corrosion system, *Corrosion Science*, **47**, 515–35.

Nicodemi, W., Mapelli, C., Venturini, R., and Riva, R., 2005, Metallurgical investigations on two sword blades of 7th and 3rd century BC found in Central Italy, *ISIJ International*, **45**(9), 1358–67.

Pense, A. W., 2000, Iron through the ages, *Materials Characterization*, **45**, 353–63.

Perttula, J., 2001, Reproduced wootz Damascus steel, *Scandinavian Journal of Metallurgy*, **30**, 65–8.

Perttula, J., 2004, Wootz Damascus steel of ancient Orient, *Scandinavian Journal of Metallurgy*, **33**, 92–7.

Raphael, K., and Tepper, Y., 2005, The archaeological evidence from the Mamluk siege of Arsuf, *Mamluk Studies Review*, **9**, 85–100.

Roll, I., 1999, Introduction: history of the site, its research and excavations, in *Apollonia–Arsuf: final report of the excavations, vol. I: the Persian and Hellenistic periods (with appendices on the Chalcolithic and Iron Age II remains)* (O. Roll and O. Tal), Monograph Series of the Institute of Archaeology 16, Tel Aviv University, Tel Aviv.

Roll, I., 2008, Der frühislamische Basar und die Kreuzfahrerburg in Apollonia–Arsuf, in *Burgen und Städte der Kreuzzugszeit* (ed. M. Piana), 252–62, Michael Imhof Verlag, Petersberg.

Schwertmann, U., and Cornell, R. M., 2000, *Iron oxides in the laboratory*, Wiley-VCH, Weinheim.

Tal, O., and Roll, I., 2011, Arsur: the site, settlement and Crusader castle, and the material manifestation of their destruction, in *The last supper at Apollonia: the final days of the Crusader castle in Herzliya* (ed. O. Tal), 8–51, Eretz Israel Museum, Tel Aviv.

Tylecote, R. F., 1962, *A history of metallurgy*, 2nd edn, The Metals Society, London.

Tylecote, R. F., and Black, J. W. B., 1980, The effect of hydrogen reduction on the properties of ferrous materials, *Studies in Conservation*, **25**, 87–96.

Wadsworth, J., and Lesuer, D. R., 2000, Ancient and modern laminated composites—from the great Pyramid of Gizeh to Y2K, *Materials Characterization*, **45**, 289–313.

Yoshikawa, H., Gunji, E., and Tokuda, M., 2008, Long term stability of iron for more than 1500 years indicated by archaeological samples from the Yamato 6th Tumulus, *Journal of Nuclear Science*, **379**, 112–17.